ACS APPLIED MATERIALS & INTERFACES

www.acsami.org

Research Article

High Catalytic Activity of Fluorophore-Labeled Y-Shaped DNAzyme/3D MOF-MoS_2NBs as a Versatile Biosensing Platform for the Simultaneous Detection of Hg^{2+}, Ni^{2+}, and Ag^{+} Ions

Rajaji Pavadai, Arunjegan Amalraj, Sivanesan Subramanian, and Panneerselvam Perumal*

Cite This: *ACS Appl. Mater. Interfaces* 2021, 13, 31710–31724

Read Online

ACCESS | Metrics & More | Article Recommendations

ABSTRACT: In this study, we have designed a three-fluorophore-labeled Y-shaped DNAzyme with a high catalytic cleavage activity and a three-dimensional (3D) MOF-MoS_2NB (metal–organic framework fused with molybdenum disulfide nanobox), which was synthesized as an efficient quencher of the fluorescent biosensor. The synthesized porous 3D MOF-MoS_2NBs and Y-shaped DNAzyme exhibited a good analytical response toward the simultaneous multiple detections of Hg^{2+}, Ni^{2+}, and Ag^{+} ions over the other coexisting metal ions. More specifically, the three kinds of enzyme aptamer and substrate aptamer (SA) were hybridized and annealed to form the Y-shaped DNAzyme structure and labeled with three different fluorophores such as FAM, TAMRA, and ROX over the 3′-end of SA. When the targets were induced, the DNAzyme was triggered to cleave the fluorophore-labeled SAs. Then, the cleaved SAs (FAM-SA, TAMRA-SA, and ROX-SA) were adsorbed on the 3D MOF-MoS_2NB surface to quench the fluorescence signal due to a noncovalent interaction (van der Waals and $\pi-\pi$ stacking interaction), which transmuted the fluorescence on-state to off-state. As a result, the fluorescence assay confiscated the high selectivity and sensitivity for the target analytes of Hg^{2+}, Ni^{2+}, and Ag^{+} ions achieved for the detection limits of 0.11 nM, 7.8 μM, and 0.25 nM, respectively. Accordingly, the sensitivity of the developed sensor was explored with a better lower detection limit than the previously reported biosensors. The utility of the designed Y-shaped DNAzyme may find a broad field of application in real water sample analysis with interfering contaminants.

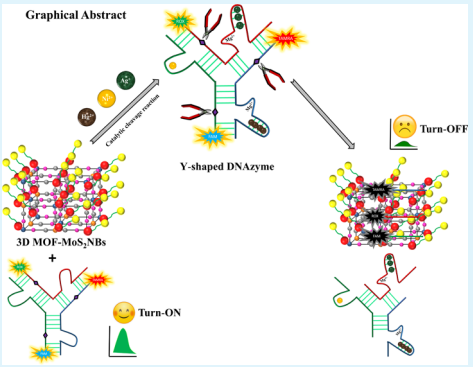

KEYWORDS: *3D MOF-MoS_2NBs, Y-shaped DNAzyme, mercury, nickel, silver, biosensor*

1. INTRODUCTION

Recently, the increasing threat of chemical pollutants in the aquatic systems has become a critical issue. The major water pollutants, especially Hg^{2+}, Ni^{2+}, and Ag^{+} ions, are the most toxic and hazardous to human health due to their strong affinity with different bio-macromolecules. The excessive accumulation of Hg^{2+}, Ni^{2+}, and Ag^{+} ions in humans has resulted in a wide range of diseases such as brain dysfunction, liver, kidneys, Minamata diseases, and neurodevelopment disorders in children. The anthropic sources, incineration of solid waste, metal smelting, and combustion of fossil fuels result in skin allergies, dermis, cancer, lung fibrosis, and disorders in the respiratory, central nervous, and cardiovascular systems.[1−3] As a result, many researchers have concentrated on the detection of single and dual heavy metal ions. However, the simultaneous detection of multiple ions is one of the hottest subjects in the field of water pollution monitoring. Therefore, from the practical application perspective, it is significant to establish effective and sensitive methods for the simultaneous detection of multiple heavy metal ions, which remains a critical issue.

Many efforts were extensively developed for the detection of Hg^{2+}, Ni^{2+}, and Ag^{+} ions, including flame atomic absorption spectroscopy, cold vapor atomic fluorescence spectroscopy, cold vapor atomic absorption spectroscopy, solid-phase microextraction coupled with high-performance liquid chromatography, atomic absorption spectroscopy, inductively coupled plasma atomic emission spectroscopy, and inductively coupled plasma mass spectroscopy.[4−11] Nevertheless, these methods possess drawbacks which include complicated operation techniques, expensive instruments, and so forth. In particular, the fluorescent sensor exhibits convenient advantages such as metal ion detection with remarkable superiority, sensitivity, low cost, easy operation, and efficiency. The

Received: April 17, 2021
Accepted: June 21, 2021
Published: July 2, 2021

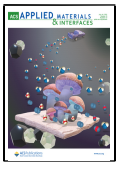

fluorescent sensors have attracted extensive attention.[12,13] A number of fluorescent biosensors for heavy metal detection are reported over the past several years.[14,15] However, sensitive and selective fluorescent sensors for multiple detections of Hg^{2+}, Ni^{2+}, and Ag^{+} ions are scarce. Frequently, significant practical limitations of Hg^{2+}, Ni^{2+}, and Ag^{+} ions are seen, which include detailed synthesis schemes, high-cost methods, and insufficient selectivity.

The catalytic DNA sequences are DNAzymes that are isolated by the systematic evolution of ligands with the help of the exponential enrichment procedure. The DNAzymes have significant advantages such as high programmability, stability, and high affinity to metal ions which can be easily modified and labeled.[16] The DNAzymes are highly catalytic oligonucleotides that require metal ions for the cleavage activity. Recently, many methods were extensively developed to obtain different DNAzymes to detect several metal ions with the help of a specific cleavage activity.[17,18] Moreover, the interest has been evinced in the development of DNAzymes functionalized with various quenching nanomaterial (labeled or unlabeled)-based fluorescent biosensors.[19−21] Specifically, this type of sensor complies with a fluorescence resonance energy transfer (FRET) mechanism, which relies on the fluorescence quenching fluorophores and quenching materials. This type of quenching material-based biosensors can effectively quench the fluorophores, eliminating the selection issues of fluorescence quencher pairs and further improving the signal-to-noise ratio of the aptamers compared to other various sensing signaling transduction techniques, namely, electrochemiluminescence, colorimetry, electrochemistry, and Raman methods.[22−24] The developed DNAzyme-based fluorescent biosensor utilizes FRET between the fluorophore (donor) and the suitable quenching materials (acceptor). Therefore, new kinds of quenching nanomaterials are established to enhance the sensing ability.

Recently, the countless well-designed metal−organic framework (MOF) has been found to be effective in the coordination of the polymeric nanoscale materials, which have drawn more attention as effective quenching materials. This framework finds a wide range of applications, which includes hydrogen storage, water splitting, proteins, gas storage, antibiotics, carbohydrates, and so forth. Thus, the MOF has become a vital research field that has encouraged many chemists and material scientists due to their unique properties such as versatile surface area, water-dispensability, tunable nature, biocompatibility, low cost, controllable shape, ultrahigh porosity, and high fluorescence quencher.[25−27] Moreover, the MOF composition exhibits various morphologies (such as nanosheets, cages, tubes, rods, cube, and so on), which can be effortlessly tuned based on the selection of various organic linkers and metal ions.[28−31] In addition, the transition metal dichalcogenides (MoS_2, WS_2, etc.) have also attracted significant attention for the effective fluorescence biosensing platforms to function as fluorescence quenchers for the detection of metal ions and biomolecules.[32,33] At present, we have aimed to incorporate the MOF (Ni−Co-based Prussian blue analogues) and MoS_2, which will enhance the biocompatibility and biodegradability. The MOF facilitates excellent electron acceptors for improving the quenching efficacy due to the $\pi-\pi$ stacking along with the van der Waals interaction.[34,35] Therefore, we have prepared the MOF fused with molybdenum disulfide nanoboxes (MOF-MoS_2NBs) for fabricating the new DNAzyme-based fluorescent biosensors for the sensitive and selective detection of the multiple metal ions.

In this investigation, we have designed the Y-shaped DNAzyme/3D MOF-MoS_2NB, which functions as a superior fluorescent sensing platform for the simultaneous detection of multiple target Hg^{2+}, Ni^{2+}, and Ag^{+} ions in a homogeneous solution. Each DNAzyme was made using an individual enzyme aptamer (EA) and a fluorophore-labeled substrate aptamer (SA). The complementary interactions between the three DNA sequences enabled hybridization with each other and the formation of a Y-shaped DNAzyme structure. Therefore, the developed Y-shaped DNAzyme structure, which primarily consisted of a double-stranded DNA, was firmer and had a very poor binding affinity with the MOF-MoS_2NBs. Upon the addition of target metal ions, the fluorophore-labeled SA was cleaved at the RNA site. In the meantime, the cleaved fluorophore-labeled SA was adsorbed onto the versatile MOF-MoS_2NB surface due to the van der Waals and $\pi-\pi$ stacking interactions (between the MOF-MoS_2NBs and nucleobases), which resulted in the quenching of the fluorescence (turn-on to turn-off). Accordingly, this fluorescent biosensing platform permits the simultaneous quenching of the three kinds of fluorescence in a SA, resulting in the multiple detections of metal ions in a homogeneous solution with excellent sensitivity. Finally, the research explores the challenges and opportunities in the field of biosensors, which is based on a complex of Y-shaped DNAzymes with MOF-MoS_2NB sensing probes. The biosensors are predicted to offer a quantitative readout of the target multiple metal ions in the real sample analysis.

2. EXPERIMENTAL SECTION

2.1. Chemicals and DNA Sequences. All the reagents and solvents used in this experiment were bought commercially. Sodium citrate, potassium acetate, ammonium molybdate, thiourea, potassium hexacyanocobaltate(III), ethanol, tris (hydroxymethyl) aminomethane, metal halides, and metal nitrates (lead nitrate, cobalt nitrate, nickel nitrate, zinc nitrate, silver nitrate, ferric nitrate, copper chloride, calcium chloride, ferrous chloride, manganese chloride, magnesium chloride, cadmium chloride, and barium chloride) were purchased from Sigma-Aldrich and Alfa Aesar. The DNA oligomers (three kinds of the fluorophore-labeled three SAs and label-free EAs) were procured from Allied Scientific Products (Kolkata, India). The sequence is given as follows.

Substrate aptamers. SA1 = TAMRA: 3′-AGGTAGAGATArAGGAAGATCCGCTG-5′

SA2 = ROX: 3′-CTCTCGAGACACTATrAGGAAGATCCGGAA-5′

SA3 = FAM: 3′-GTGCAGGTAGAGAAGGrATATCACTCA-5′

Enzyme aptamers

EA1 = 5′-CACGTCCATCTCTTCAGT(C)5CGGAAACG(C)5ACAGCGTACCCTGAACATAGTGAGT-3′

EA2 = 5′-GAGAGCTCTCTTTCTCTCATAGCTTCTAGGCCTT-3′

EA3 = 5′-CACGTCCATCTCTTCAGT(T)5CGGAAACG(T)5ACAGCGTACCCTGAACATAGTGAGT-3′

The stock solution of DNAs was prepared using Tris−HCl (pH 8.0). All of the chemical reagents were of analytical grade and used directly as collected without any purification.

2.2. Structural Characterization. The fluorescence emission spectra were obtained using a HORIBA JOBIN YVON Fluoromax-4 Spectrofluorometer with a xenon lamp excitation source with excitation wavelengths of 491, 575, and 554 nm and emission wavelengths of 523, 606, and 572 nm, respectively, and a slit width of 5 nm. High-resolution scanning electron microscopy (HR-SEM, Thermo scientific Apreo S) was used. The HR transmission electron

https://doi.org/10.1021/acsami.1c07086
ACS Appl. Mater. Interfaces 2021, 13, 31710−31724

Scheme 1. Schematic Diagram for the Synthesis of MOF-NBs

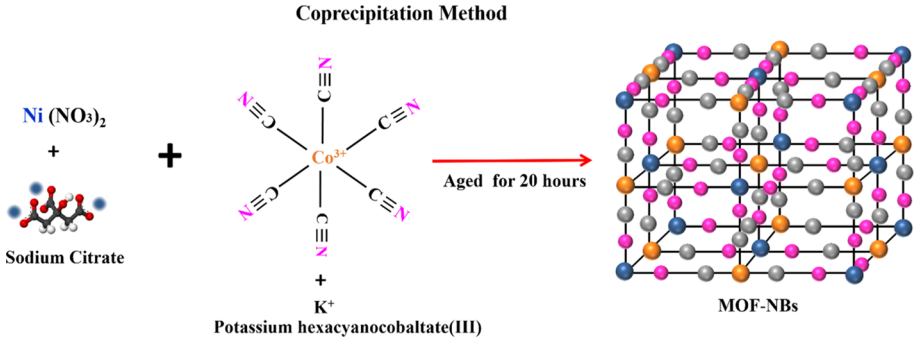

Scheme 2. Schematic Diagram for the Synthesis of MOF-MoS_2NBs

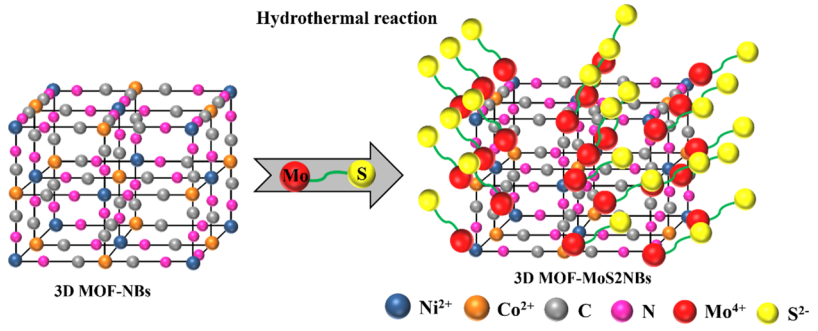

Scheme 3. Schematic Diagram for Three Kinds of Fluorophore-Labeled Y-Shaped DNAzymes

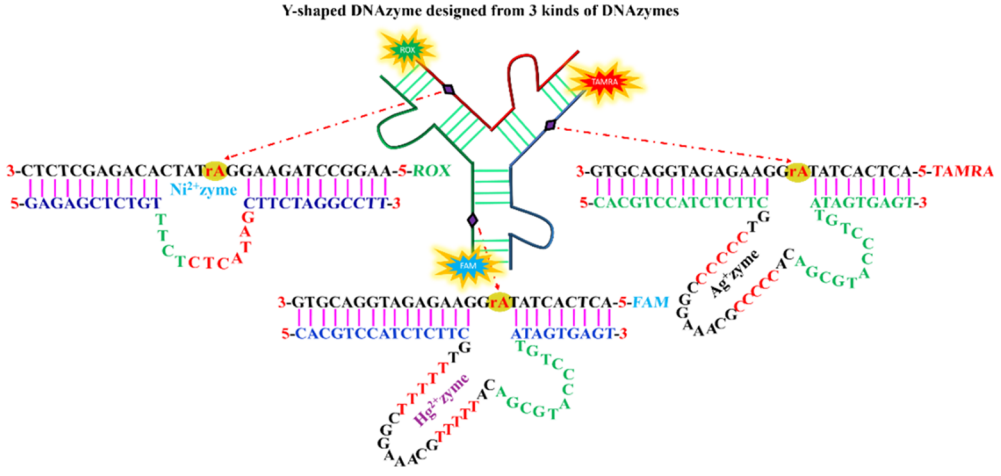

microscope was a JEOL Japan, JEM-2100 Plus, which was operated at 200 kV. The elemental mapping was also conducted with the electron microscope for HR-SEM equipped with the energy-dispersive X-ray spectroscopy (EDXS) of ISIS300 (Oxford) to identify the distribution of Ni, Co, Mo, S, C, N, and O profiles on the surface of the MOF-MoS_2NBs. The Fourier transform infrared (FTIR) spectra of the solid sample embedded in the KBr pellets were collected with the help of Agilent Technologies at room temperature. The X-ray diffraction (XRD) spectrum was recorded using a PAN analytical X'pert pro-X-ray diffractometer with Cu Kα radiation. In addition, X-ray photoelectron spectroscopy (XPS, PerkinElmer Phi 1600 ESCA system), using Mg (1486.6 eV) as the radiation source, was used to estimate the surface element composition, element-binding configuration, and charge compensation of the MOF-MoS_2NBs. Moreover, circular dichroism spectroscopy (CDS) was carried out for the Y-shaped DNAzyme creation. The three kinds of EA and SA were mixed to 4 μM in 10 mM Tris−HCl (pH 7.0) without any Hg^{2+}, Ni^{2+}, and Ag^{+} ions. CDS was performed in the range between 230 and 300 nm using a JASCO J-815 spectrometer (JASCO International Co. Ltd., Japan) under the following conditions: room temperature with a 1 × 1 cm quartz cuvette, data interval: 1 nm, bandwidth: 2 nm, scan speed: 50 nm/min, and response time: 5 s. Hg^{2+}, Ni^{2+}, and Ag^{+} were dissolved in deionized water (DW), and the final concentration was realized by adding 100 μL of cation solution to the 1.9 mL Y-shaped DNAzyme solution.

2.3. Preparation of Quenching Nanomaterials. *2.3.1. Synthesis of MoS_2-NSs.* For a typical synthesis,[36] 700 mg of Na_2MoO_4, 800 mg of CH_4N_2S, and 100 mg of polyethylene glycol (MW ≈ 2000) were dissolved in 35 mL of DW and vigorously stirred for 12 h to get a homogeneous suspension. The obtained mixture was poured into a Teflon-lined stainless steel autoclave and kept at 200 °C in an oven for 24 h. After cooling, the black powders were collected, and unreacted reactants were removed by repeated centrifuging in ethanol and water. Finally, the resulting MoS_2 nanosheet was dried at 70 °C for 12 h.

https://doi.org/10.1021/acsami.1c07086
ACS Appl. Mater. Interfaces 2021, 13, 31710−31724

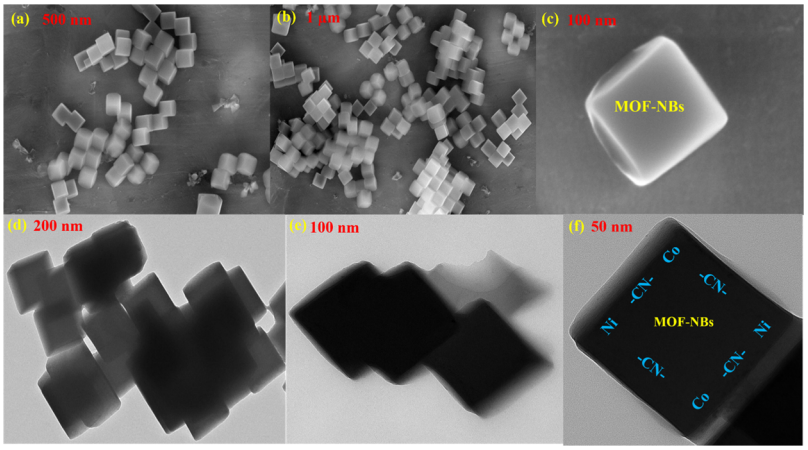

Figure 1. HR-SEM (a–c) and HR-TEM (d–f) images of MOF-NBs.

2.3.2. Synthesis of MOF-NBs. The MOF-NBs (Scheme 1) were prepared using a modified precipitation method.[37] In a typical preparation, 0.0004 M nickel nitrate and 0.0007 M sodium citrate were dissolved in 15 mL of DW. Subsequently, 0.2 M potassium hexacyanocobaltate(III) was dissolved in 15 ml of DW. The two solutions were mixed using magnetic stirring for 4 min at room temperature. The obtained mixed solution was aged for 20 h at room temperature. The required product was centrifuged, and the precipitates were washed with H_2O/C_2H_5OH and dried at 65 °C overnight.

2.3.3. Synthesis of MOF-MoS_2NBs. 60 mg of as-prepared MOF-NBs and 30 mg of MoS_2-NSs were dissolved in 60 mL of *N,N*-dimethylformamide (DMF) with the help of ultrasonication for 25 min. Then, the blends were transferred to a 100 mL Teflon-lined stainless steel autoclave and heated to 215 °C for 20 h.[38] After that, the mixture was cooled to room temperature. The transparent and colorless crystals were filtered off, and the blends were washed several times using deionized H_2O/C_2H_5OH and dried at 65 °C. The obtained product was denoted as "MOF-MoS_2NBs" (Scheme 2).

2.4. Design for the Y-Shaped DNAzyme and Detection Procedure. The preparation of a Y-shaped DNAzyme involves the hybridization of 5 μL of 2 μM SAs and 10 μL of 2 μM EAs (Hg^{2+}-zyme) in a buffer (50 mM Tris–HCl, 50 mM NaCl, pH = 8.0) at 37 °C for 30 min. The same procedure was followed to prepare two more DNAzymes (Ni^{2+}-zyme and Ag^{+}-zyme). After annealing, the three separate DNAzymes were added and kept for 1 h to generate the Y-shaped DNAzyme (Scheme 3). The detailed procedure for the detection of multiple targets is as follows: 10 μL of Y-shaped DNAzyme, 800 μL of buffer, 50 mM Tris–HCl (50 mM NaCl, pH = 8.0), and 80 μL of MOF-MoS_2NBs (25 $\mu g \cdot mL^{-1}$) were sequentially added into a plastic centrifuge tube. After 30 min of reaction, the solution was transferred into a cuvette. Subsequently, the freshly prepared 10 μL of the target stock solution was added in different concentrations and incubated for 25 min. The fluorescence intensity was measured using the respective excitation and the emission wavelength of the three fluorophores.

2.5. Detection of Real Samples. The real water samples are used to prove the feasible development of our technique. To determine the presence of Hg^{2+}, Ni^{2+}, and Ag^{+}, the real water samples were calibrated at 8.0 pH. This was followed by filtration using a 0.22 μM membrane filter for isolating the insoluble impurities. These samples were collected from the SRM Institute campus, Chennai, India. The different concentrations of Hg^{2+} (0.3, 0.6, and 0.9 nM), Ni^{2+} (10, 15, and 20 μM), and Ag^{+} (0.4, 0.8, and 1.2 nM) ions were spiked in the RWS. The fluorescence studies of these samples were analyzed using the designed Y-shaped DNAzyme/MOF-MoS_2NB biosensor.

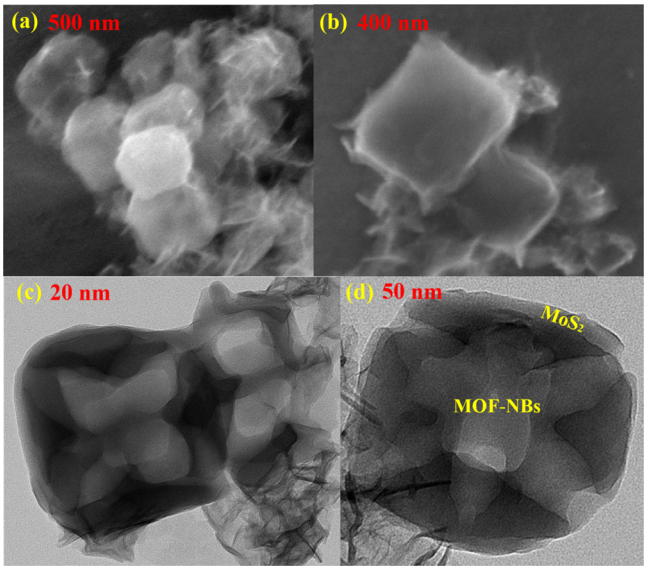

Figure 2. HR-SEM (a,b) and HR-TEM (c,d) images of MOF-MoS_2NBs.

3. RESULTS AND DISCUSSION

3.1. Material Characterization. The surface morphologies of the MOF-NBs and MOF-MoS_2NBs were scrutinized with the help of HR-SEM and HR transmission electron microscopy (HR-TEM). Figure 1 shows the HR-SEM and HR-TEM images, which reveals the high uniformity of the as-prepared MOF-NBs with an average particle size of about 320 nm, which displayed cubic-like crystal lattices consisting of a large number of cubic formations. Furthermore, the MoS_2 incorporated with the MOF-NBs was coordinated on the outer surface of the MOF-NBs to form MOF-MoS_2NBs. The HR-SEM and HR-TEM (Figure 2) images of MOF-MoS_2NBs clearly reveal that the thin nanosheets of the MoS_2 were successfully grown on the surface of the MOF-NBs. However, the MOF-MoS_2NBs were seen to retain the original cubic structure. From the experimental results, it is clear that the MOF-MoS_2NBs were suitable as a fluorescence quencher, and they would be able to bind the DNA with the help of $\pi-\pi$ stacking and van der Waals interaction. Furthermore, EDXS scans indicated that the MOF-NBs have Ni, Co, C, and N elements, which are shown in Figure 3a. In addition, the molybdenum (Mo), sulfur (S), and oxygen (O) elements were

https://doi.org/10.1021/acsami.1c07086
ACS Appl. Mater. Interfaces 2021, 13, 31710–31724

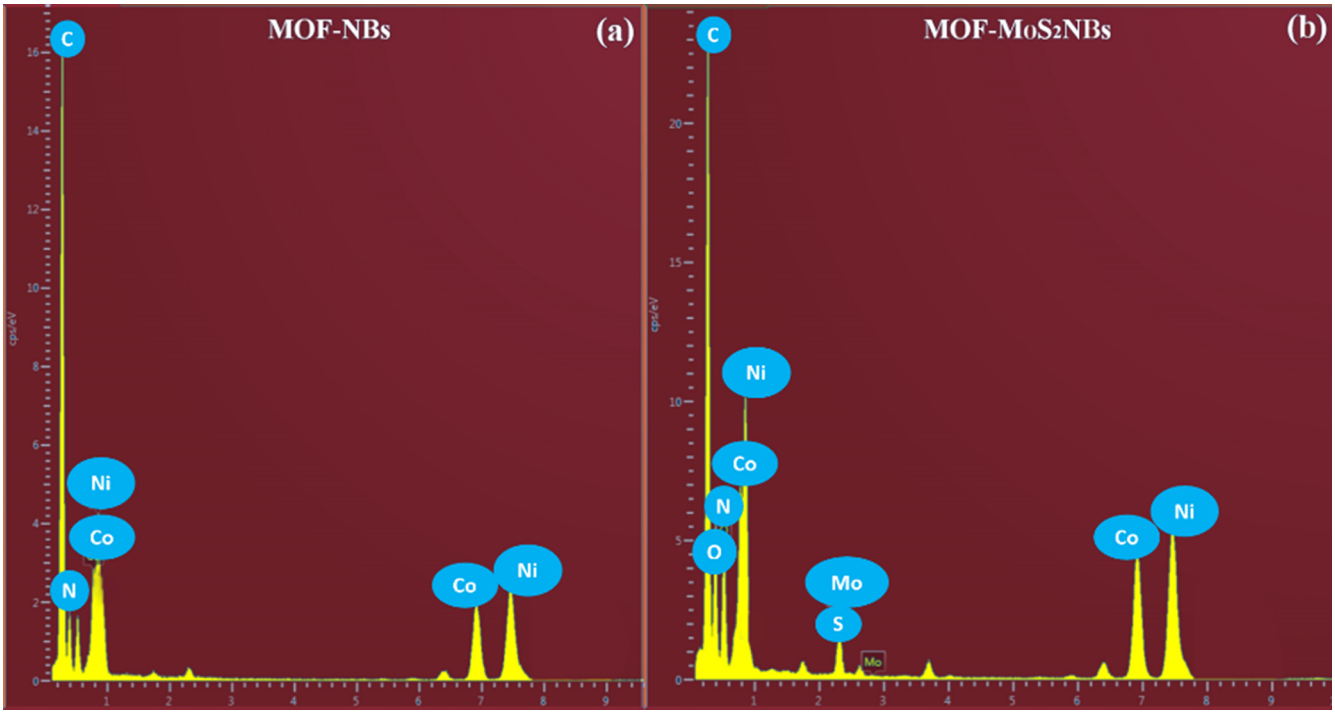

Figure 3. EDXS for (a) MOF-NBs and (b) MOF-MoS_2NBs.

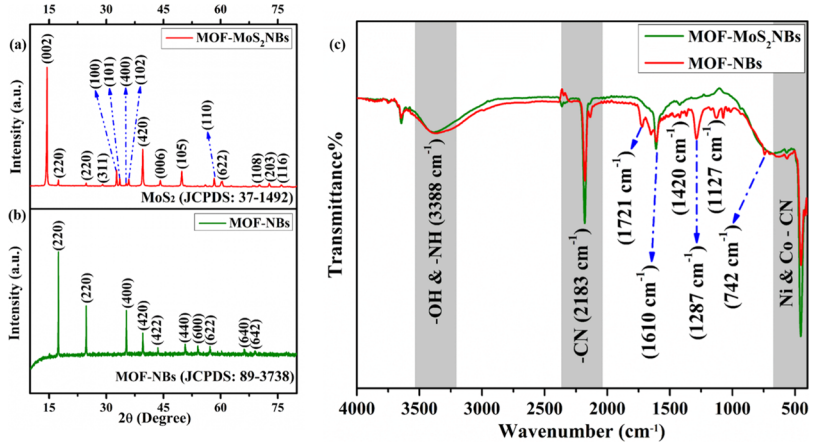

Figure 4. XRD (a,b) and FT-IR (c) spectra for MOF-NBs and MOF-MoS_2NBs.

present in the MOF-MoS_2NBs (Figure 3b). Therefore, we conclude that the MoS_2 nanosheets were successfully incorporated into the pores and cubic surfaces of the MOF-NBs.

To identify the crystalline nature, the chemical composition and oxidation state of the MOF-NBs and MOF-MoS_2NBs were procured using XRD, FTIR, EDXS, and XPS. Figure 4a,b shows the XRD spectra, which can be seen as well indexed with the face-centered cubic phase (JCPDS 89-3738).[39] In these spectra, the two samples were indexed with (17.5°-200), (24.8°-220), (35.4°-400), (39.7°-420), (43.7°-422), (50.9°-440), (54.2°-600), (57.4°-620), (66.4°-640), and (69.3°-642) planes, respectively. All the diffraction peaks correspond to the pure cubic MOF-MoS_2NBs with no additional peaks from impurities. According to the crystal field theory, the crystal structure of MOF-NBs possesses high-spin Ni ions which are coordinated with nitrogen atoms, and the low-spin Co ions are coordinated with carbon atoms, resulting in the formation of a three-dimensional network with Ni^{2+}−NC−Co^{3+} chains. In divergence to MOF-NBs, several peaks were perceived. For example, the peaks were seen at (14.3°-002), (29.0°-311), (32.6°-100), (33.5°-101), (35.8°-102), (44.1°-006), (49.8°-105), (58.3°-110), (70.1°-108), (72.7°-203), and (75.9°-116) in the MOF-MoS_2NBs, which corresponded to MoS_2. Also, few other peaks were observed, which were related to NiS.[40,41] Furthermore, the chemical bonding confirmation of the metal ion immobilization and the metal sulfide functionalization was successfully assigned to the surface of the MOF-NBs and the MOF-MoS_2NBs, whose results are shown in Figure 4c. The MOF-NBs and MOF-MoS_2NBs exhibit a high-intensity peak, which was at 2183 cm^{-1}. This was attributed to the CN stretching vibration of the Ni^{2+}−CN−Co^{3+} complex, and the bands at 562 and 453 cm^{-1} are ascribed to the metal cyanide (Co−CN and Ni−CN).[42] In contrast, the MOF-MoS_2NBs revealed peaks at 1721 cm^{-1} and 742 cm^{-1} for the Mo−O and Mo−S vibrations, respectively (metal sulfide). From MoS_2, the

https://doi.org/10.1021/acsami.1c07086
ACS Appl. Mater. Interfaces 2021, 13, 31710−31724

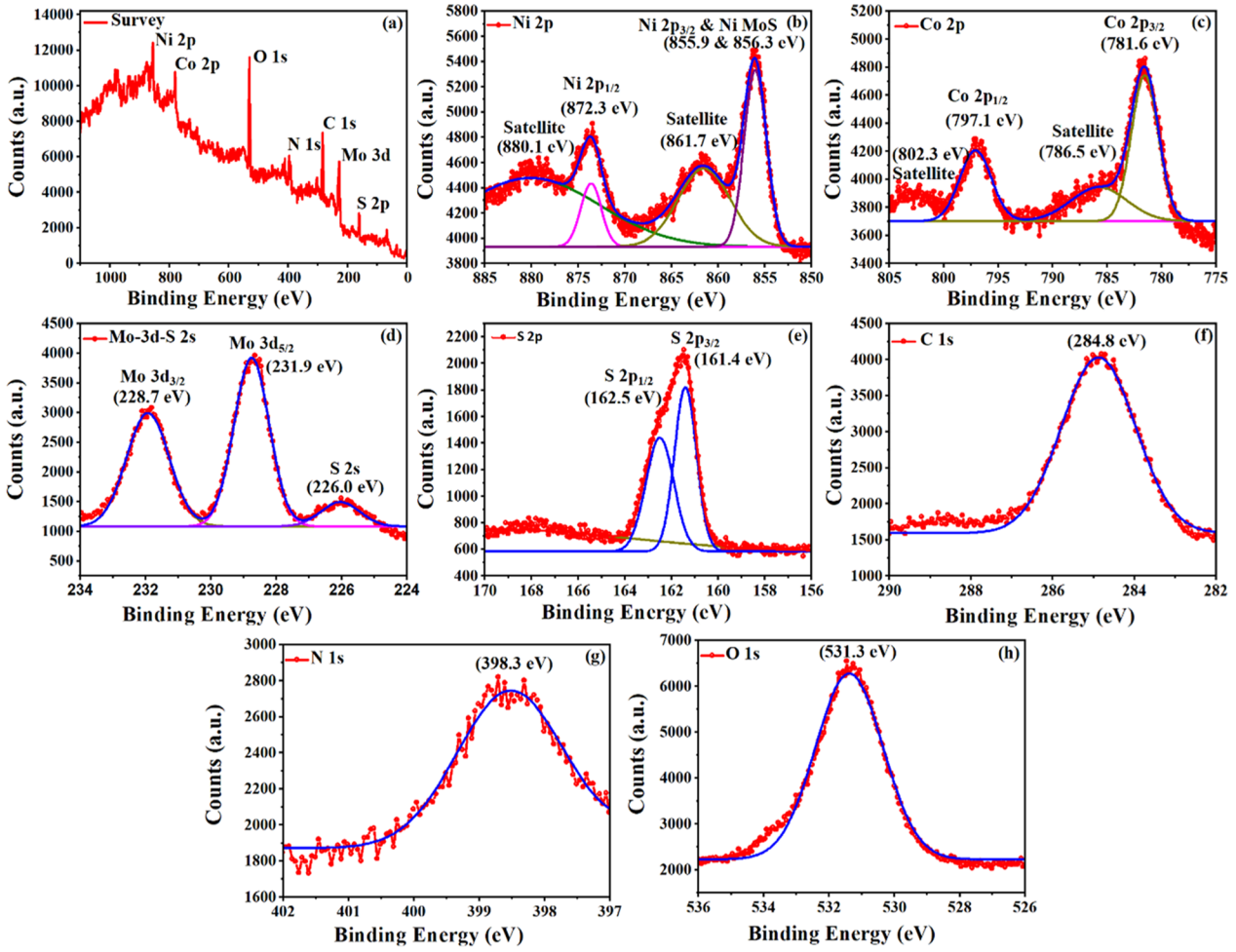

Figure 5. XPS of MOF-NBs and MOF-MoS_2NBs: (a) survey, (b) Ni 2p, (c) Co 2p, (d) Mo-3d-S 2s, (e) S 2p, (f) C 1s, (g) N 1s, and (h) O 1s.

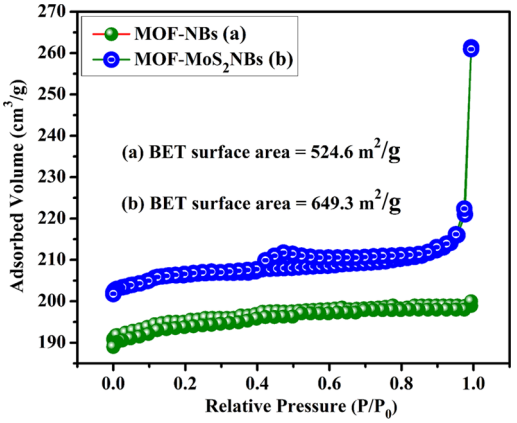

Figure 6. BET analysis for (a) MOF-NBs and (b) MOF-MoS_2NBs.

N-dimethylformamide moiety peak at 1610 cm^{-1}(C═O) and the OH/NH stretching broadband center at 3388 cm^{-1} were observed. The additional absorptions at 1420 cm^{-1} (vC═S), 1287¯, and 1127 cm^{-1} (vC−N) were assigned to MoS_2. This peak revealed the thiourea of the MoS_2 surface. Therefore, the conclusions strongly suggest that Mo−S_2 was well incorporated on the versatile MOF-NB surface.

The XPS measurements were performed to confirm the chemical state and elemental composition of the prepared MOF-MoS_2NBs. The outcomes are revealed in Figure 5a−h. In Figure 5a, the spectrum of the MOF-MoS_2NBs confirmed the presence of Ni 2p, Co 2p, Mo 3d, S 2s, S 2p, N 1s, O 1s, and C 1s without impurities. The Ni $2p_{3/2}$ spin−orbit peaks at 855.9 eV correspond to Ni in the Ni−MoS and Ni $2p_{1/2}$ spin−orbit peaks at 872.3 eV, as shown in the Ni 2p spectra (Figure 5b),[43] while a peak of 856.3 eV contributes to the Ni^{2+} species. The additional peaks at 861.7 and 880.1 eV can be ascribed to the relating Ni species' satellite points. In Co 2p, the XPS spectra (Figure 5c) show the two distinct peaks centered at 797.1 and 781.6 eV, which are assigned to the Co $2p_{1/2}$ and the Co $2p_{3/2}$ spin−orbit peaks, respectively. Additionally, the satellite bands at 802.9 and 789.7 eV were attributed to the Co species. Also, the spectrum of Mo 3d-S 2s at the peak of 226 eV relates to the S 2s species (Figure 7d).[44] Furthermore, Mo^{4+} is being attributed to the two major peaks at 228.7 and 232.3 eV, and the other peak at 226 eV consists of S 2s. The two peaks located at 161 and 162 eV in the S 2p spectrum (Figure 5e) correspond to the S $2p_{3/2}$ and S $2p_{1/2}$ orbitals of S^{2-}. Consequently, the C 1s high-resolution spectrum of the MOF-MoS_2NBs (Figure 5f) could be curve-fitted with one peak component, and it contains a binding energy of 284.8 eV for the C−N species. Also, the N 1s spectra (Figure 5g) had one peak at 398.3 eV, attributing to the presence of C−N in the MOF-MoS_2NBs. In Figure 5h, the peak at 531.3 eV can be ascribed to −OH from the crystal water. These results revealed that the MoS_2 nanosheets were successfully incorporated onto the MOF-NB surface. Therefore, the prepared MOF-MoS_2NBs

https://doi.org/10.1021/acsami.1c07086
ACS Appl. Mater. Interfaces 2021, 13, 31710−31724

Scheme 4. Schematic Illustration of the Simultaneous Fluorescence Detection of Hg^{2+}, Ni^{2+}, and Ag^{+} Ions Based on the Y-Shaped DNAzyme/MOF-MoS_2NBs

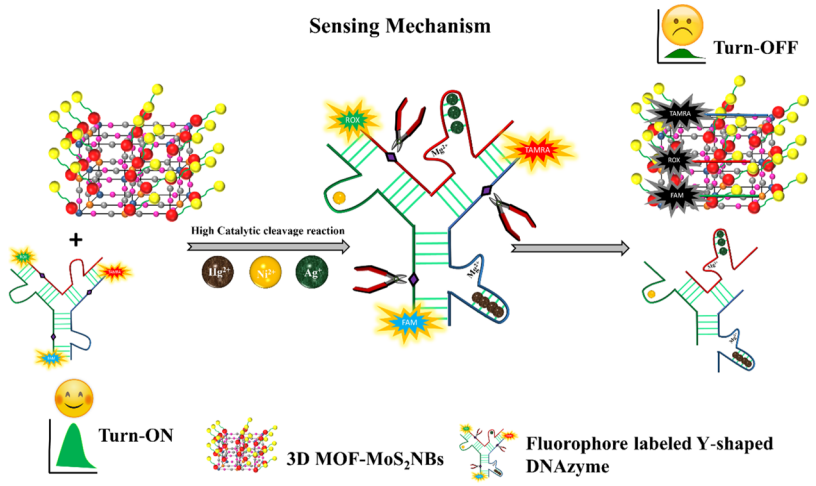

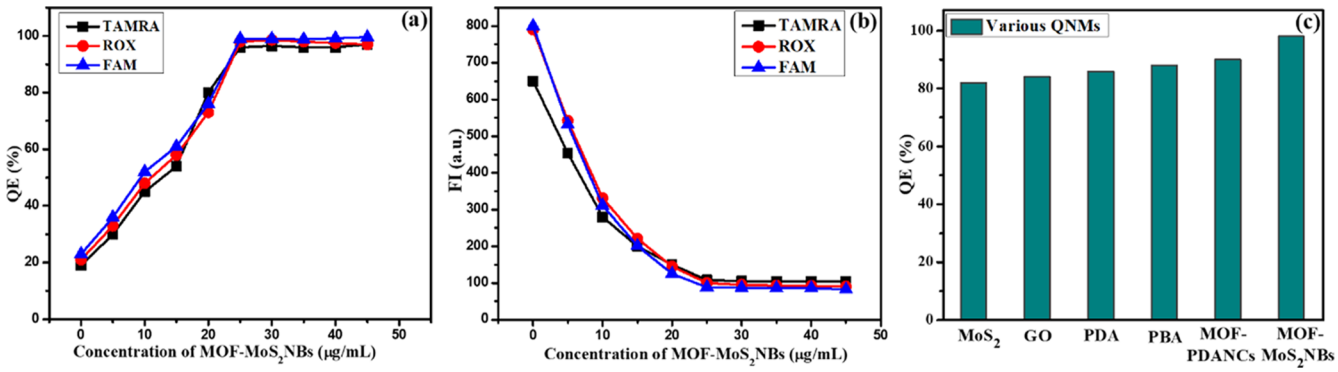

Figure 7. (a) Quenching efficiency of MOF-MoS_2NBs [100 nM Y-shaped DNAzyme in 10 mM Tris−HCl (pH 8.0) with 25 mM NaCl], (b) effects of the MOF-MoS_2NB concentration on the fluorescence intensity of FAM, ROX, and TAMRA, and (c) MOF-MoS_2NBs exhibit a high fluorescence quenching efficiency compared to other similar quenching nanomaterials (GO, PBA, MoS_2, PDA, and MOF-PDANCs).

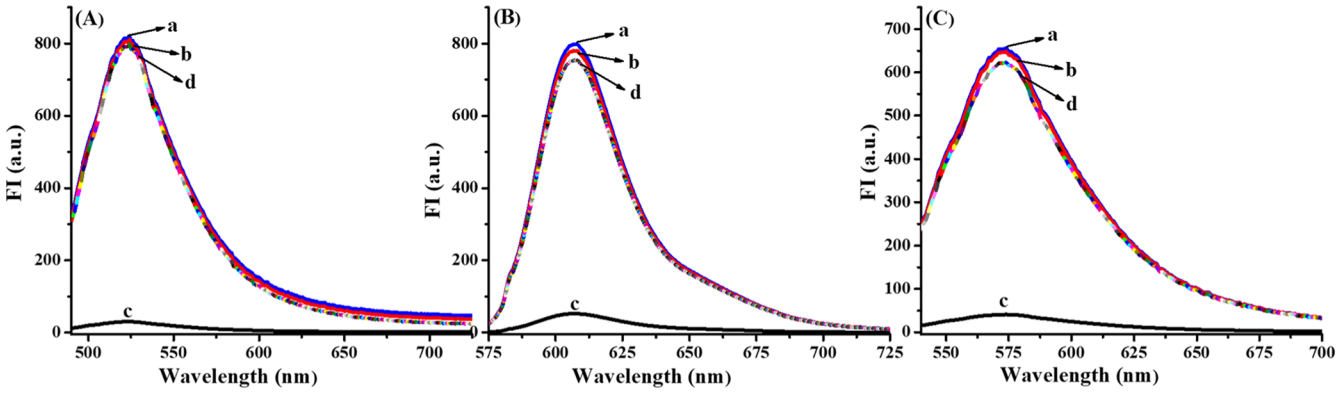

Figure 8. (A−C) Fluorescence intensity of Hg^{2+}, Ni^{2+}, and Ag^{+} ions in various conditions. [A,B,C(a)] 100 nM fluorophore-labeled Y-shaped DNAzyme. [A,B,C(b)] 100 nM Y-shaped DNAzyme with a quenching material (MOF-MoS_2NBs). [A,B,C(c)] 100 nM Y-shaped DNAzyme and target metal ions (200 nM Hg^{2+}, 300 μM Ni^{2+}, and 300 nM Ag^{+}) with MOF-MoS_2NBs. [A,B,C(d)] 100 nM Y-shaped DNAzyme and other metal ions (50 nM) with MOF-MoS_2NBs.

were selected as a highly effective DNA adsorbent and fluorescence quencher.

Furthermore, the as-prepared MOF-NB and MOF-MoS_2NB surface areas were analyzed using the nitrogen gas adsorption/desorption isotherms. As shown in Figure 6, the Brunauer−Emmett−Teller (BET) specific surface area for the MOF-NBs and MOF-MoS_2NBs were measured to be 524.6 and 649.3 m^2 g^{-1}, which was significantly larger than for the other MOF-based nanomaterials.[45−47] The high specific surface area could allow for more DNA adsorption, making the fluorescence quenching process easier.

3.2. Mechanism of the Simultaneous Detection Sensing Platform. In this sensing principle (Scheme 4), we have designed the Y-shaped DNAzyme, which is employed in a

https://doi.org/10.1021/acsami.1c07086
ACS Appl. Mater. Interfaces 2021, 13, 31710−31724

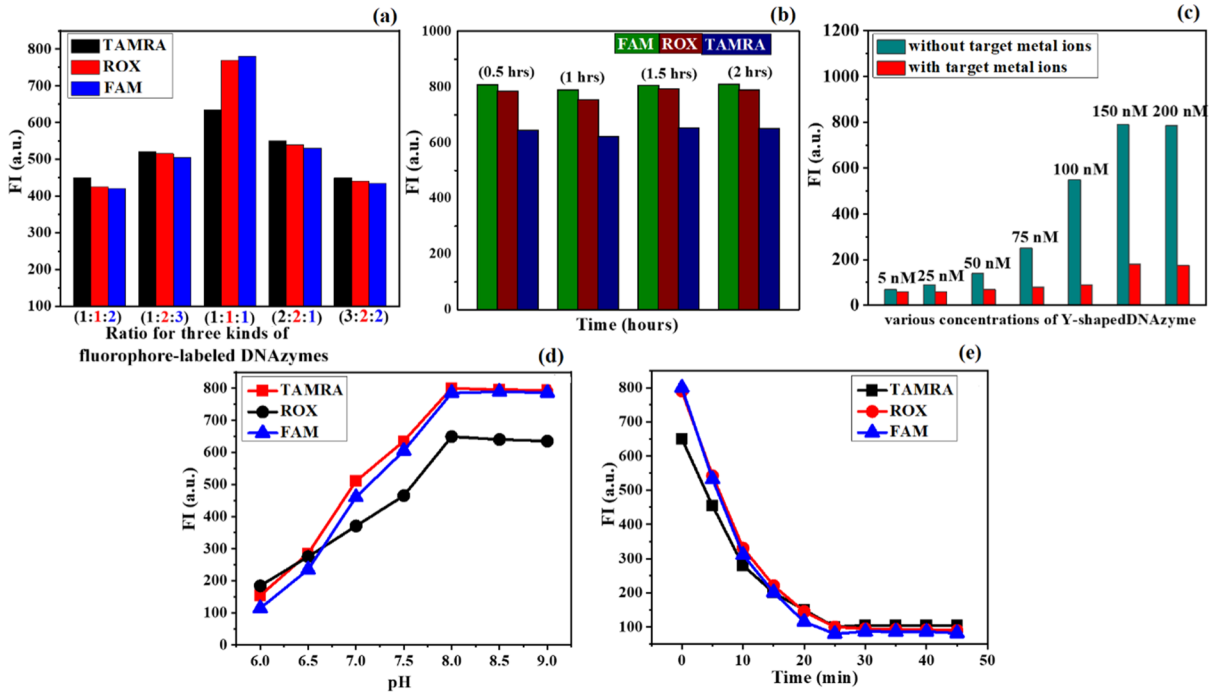

Figure 9. (a) Fluorescence stability of the Y-shaped DNAzyme structure with various ratios, (b) fluorescence stability of the Y-shaped DNAzyme with various hours, and (c) influence of DNAzyme concentration on the fluorescence intensity with 10 mM Tris−HCl (pH 8.0) with 25 mM NaCl and 25 μg/mL MOF-MoS_2NBs (200 nM Hg^{2+}). (d) Influence of pH on the DNAzyme activity with a 100 nM formed Y-shaped DNAzyme structure in 10 mM Tris−HCl with 25 mM NaCl, 25 μg/mL MOF-MoS_2NBs, 200 nM Hg^{2+}, 300 μM Ni^{2+}, and 300 nM Ag^{+}. (e) Effects of the incubation time on the fluorescence intensity with a 100 nM formed Y-shaped DNAzyme in 10 mM Tris−HCl (pH 8.0) with 25 mM NaCl and 25 μg/mL MOF-MoS_2NBs (200 nM Hg^{2+}, 300 μM Ni^{2+}, and 300 nM Ag^{+}).

fluorescent biosensor for the simultaneous detection of Hg^{2+}, Ni^{2+}, and Ag^{+}. The formation of the Y-shaped DNAzyme consists of three EA and SA portions in detail. This is because the edges of the SA portions were labeled with three different fluorophores such as FAM, TAMRA, and ROX. A unique reciprocal relationship exists between the EAs and SAs. The EA portions interact with the SA portion to form a Y-shaped DNAzyme in the process of annealing. In addition, each SA has a RNA site, which can be cleaved by the presence of specific metal ions (Hg^{2+}, Ni^{2+}, and Ag^{+}). To detect the Hg^{2+} and Ag^{+} ions, we used the Mg^{2+}zyme as Hg^{2+} and Ag^{+}zyme due to the initiation of catalytic cleavage activity by Mg^{2+}. Thus, the DNAzyme was mixed with Mg^{2+} ions, which made the DNAzyme capable of detecting the Hg^{2+} and Ag^{+} ions. In addition, the Hg^{2+} and Ag^{+} ions quickly restored the stem-loop structure and activated the DNAzyme to effectively cleave the FAM- and TAMRA-labeled SAs due to the specific affinity between the metal ions and the base pairs in the enzyme strands. For example, Hg^{2+} was strongly coordinated with the thymine base pair through T−Hg^{2+}−T and Ag^{+} was strongly coordinated with the cytosine base pairs with the help of the C−Ag^{+}−C coordination. Simultaneously, the detection of Ni^{2+} ions was done using specific DNAzymes with a small modification at RNA sites of the SA, where the RNA structure of the cleavage point was changed using the nitrogen-rich glycyl−histidine ligand. This modified cleavage point contained a carbonyl and an imidazole group, which provided multiple nickel binding sites. After adding the Ni^{2+} ion, the RNA site was cleaved to release the ROX-labeled SA. Finally, the three splintered SA fragments with fluorophores (FAM, ROX, and TAMRA) were released from the Y-shaped DNAzyme and bound with the MOF-MoS_2NBs using noncovalent interactions ($\pi-\pi$ stacking and van der Waals force). Thus, the MOF-MoS_2NBs induced the effective fluorescence quenching functionality, and the fluorescence signal was significantly decreased. Nevertheless, in the absence of target metal ions, the Y-shaped DNAzyme did not adsorb onto the surface of the MOF-MoS_2NBs. This is because the designed Y-shaped DNAzyme consisted of double-stranded DNA, which had a weak binding ability with MOF-MoS_2NBs, resulting in the absence of fluorescence reduction.

3.3. Fluorescence Quenching Performance of MOF-MoS_2NBs. Figure 7a reveals the fluorescence quenching efficiency of the MOF-MoS_2NBs. The key sensing probe of the Y-shaped DNAzyme consisted of three types of SA with attached dissimilar fluorophores such as FAM, TAMRA, and ROX. In the absence of metal ions, the fluorophore-attached Y-shaped DNAzyme probes exhibited strong fluorescence emissions at 523, 606, and 572 nm, respectively, due to the incapability of the Y-DNAzyme (it mainly happened due to the weak binding force of the dsDNA with the MOF-MoS_2NBs) to adsorb onto the MOF-MoS_2NBs. However, in the presence of the target metal ions, it triggered the RNA sites of the Y-shaped DNAzyme and cleaved the SAs. The bonding with the MOF-MoS_2NBs results in the quenching of the fluorescence signal dramatically due to the $\pi-\pi$ stacking and the van der Waals interaction between the exposed nitrogenous nucleobases and the MOF-MoS_2NBs. The as-prepared MOF-MoS_2NBs possessed a combination of two nanomaterials, namely, the MOF-NBs and the MoS_2 sheet. The MOF-NBs exhibited $\pi-\pi$ stacking and an electrostatic interaction between the aromatic nitrogenous nucleobases and the π-electrons rich in the −CN groups on the MOF-NB surface. Moreover, the adsorption of DNA onto the MOF-NB surface

https://doi.org/10.1021/acsami.1c07086
ACS Appl. Mater. Interfaces 2021, 13, 31710−31724

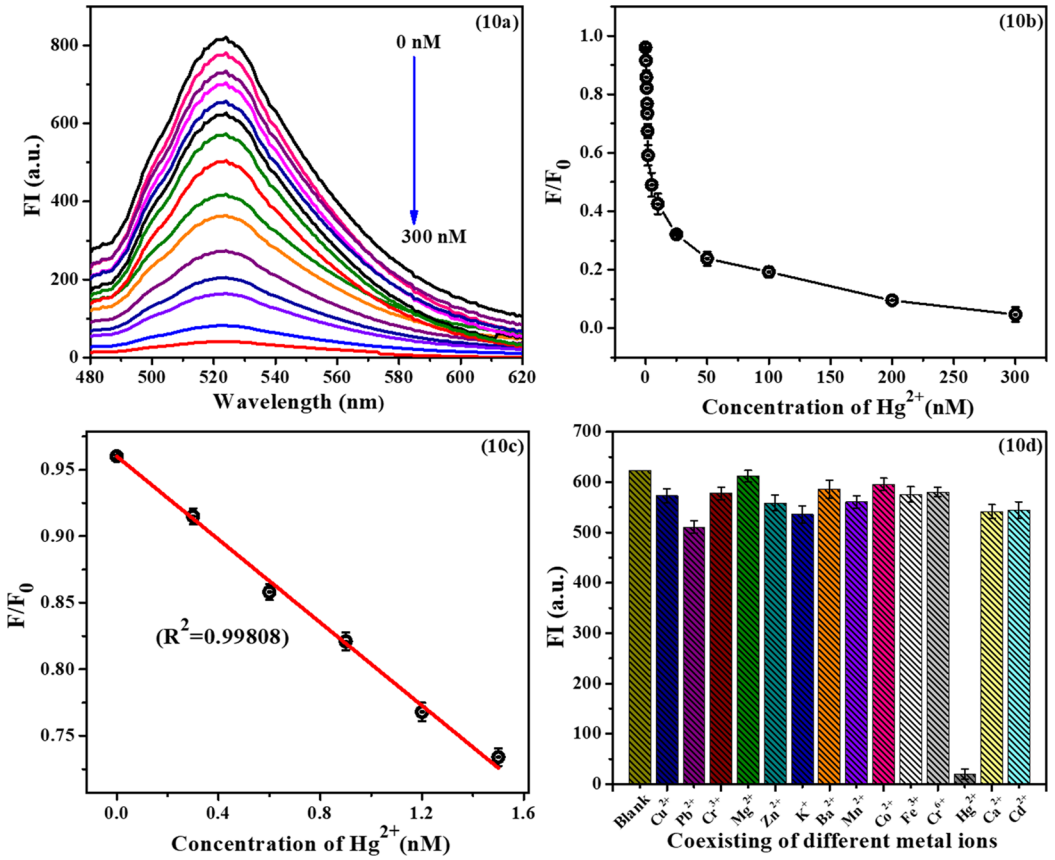

Figure 10. (a) Fluorescence spectra for Hg^{2+} MOF-MoS_2NBs (25 $\mu g \cdot mL^{-1}$) and Y-shaped DNAzyme (20 μM) at various concentrations (0, 0.3, 0.6, 0.9, 1.2, 1.5, 1.8, 2.1, 5, 10, 25, 50, 100, 200, and 300 nM) in 20 mM TRIS (pH = 8.0) at 37 °C; (b) resolution of fluorescence against the Hg^{2+} concentrations; (c) linear relationship between the fluorescence intensity and Hg^{2+} concentrations (0−1.6 nM); and (d) selectivity of Hg^{2+} (200 nM) and coexisting metal ions (400 nM). Error bars displayed the standard deviation for three individual tests.

also occurred as a result of the binding of the phosphate skeleton in the DNA to Ni^{2+} and Co^{2+} in the MOF-NBs.

The MoS_2 nanosheets exhibit a higher fluorescence quenching efficiency toward the fluorophore-labeled ssDNA. This is because MoS_2 acts as a very strong adsorbent for the ssDNA via the van der Waals interaction [significant electronegativity between Mo and S, polarized electron distribution can occur, which is beneficial for the van der Waals interactions (e.g., dipole and induced dipole interactions)] between the nucleobases and MoS_2. For example, the H atom of the CH_3 group in the adenine bases interacted with the S atom of the MoS_2 surface. For cytosine, the H atom of the CH_3 group and the O atom are quite closer to the MoS_2 surface.

The fluorescence quenching efficiency was calculated using the formula QE= $(F_P - F_{MOF}/F_P) \times 100\%$, where F_P is the fluorescence intensity of the pure fluorophore in the Y-shaped DNAzyme and F_M is the fluorescence intensity after the addition of the MOF-MoS_2NBs with the fluorophore-attached Y-shaped DNAzyme. The quenching efficiency of the various quenching nanomaterials was achieved above 95%. On the other hand, the 99.2% fluorescence quenching efficiency was achieved by 25 μg/mL MOF-MoS_2NBs (Figure 7b). Therefore, 25 μg/mL was selected as an optimized concentration for effective fluorescence quenching. The quenching efficacy of the MOF-MoS_2NBs was compared with other similar quenching nanomaterials (GO, PBA, MoS_2, PDA, and MOF-PDANCs), as revealed in Figure 7c. The experimental results of GO, PBA, MoS_2, PDA, and MOFs revealed a less quenching performance compared to the MOF-MoS_2NBs due to the rigidity and a lesser number of the surface absorbing groups.

3.4. Study for the Viability of Simultaneous Detection of Hg^{2+}, Ni^{2+}, and Ag^{+} Ions. The viability of the concurrent ultrasensitive detection of the Hg^{2+}, Ni^{2+}, and Ag^{+} ions was analyzed using various samples. As seen in Figure 8a−c, the fluorescence intensities of Figure 8A,B,C(a) are relatively high with the inclusion of the fluorophore-labeled Y-shaped DNAzyme. Figure 8A,B,C(b) reveals that the fluorescence intensities do not change clearly with the addition of the MOF-MoS_2NBs to the Y-shaped DNAzyme. However, in the inclusion of the target metal ions, the cleavage reaction can be initiated to produce three kinds of fluorophore-labeled SA fragments. The SA fragments can absorb onto the MOF-MoS_2NB surface due to the robust interaction between the MOF-MoS_2NBs and the fluorophore-labeled SA fragments, resulting in the intense quenching of the fluorescence intensities [Figure 8A,B,C(c)]. While the other metal ions were injected into the MOF-MoS_2NBs/Y-shaped DNAzyme [Figure 8A,B,C(d)], there was no fluorescence change which indicated that the other target metal ions do not cleave the RNA site.

3.5. Optimization of the Sensing System. The sensing probe conditions were optimized with various several experimental factors to achieve the best sensing performance, including the stability of the Y-shaped DNAzyme, the concentration of the Y-shaped DNAzyme, the effect of reaction

https://doi.org/10.1021/acsami.1c07086
ACS Appl. Mater. Interfaces 2021, 13, 31710−31724

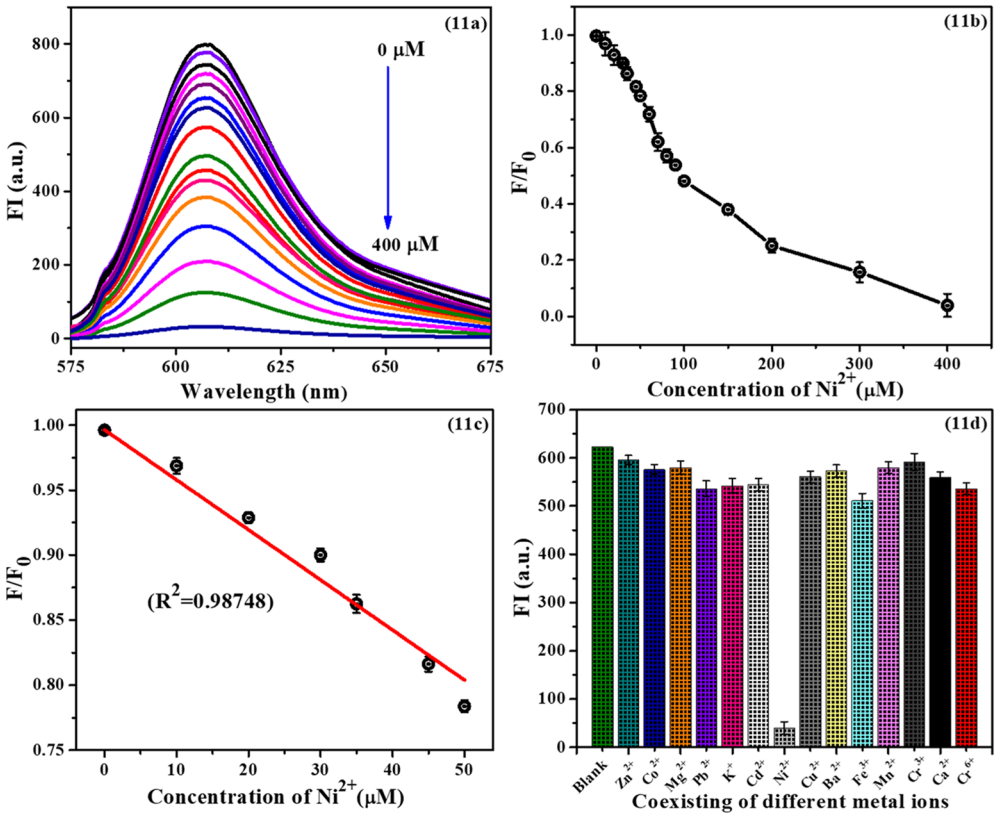

Figure 11. (a) Fluorescence spectra for Ni^{2+} MOF-MoS_2NBs (25 $\mu g \cdot mL^{-1}$) and Y-shaped DNAzyme (20 μM) at various concentrations (0, 10, 20, 30, 35, 40, 45, 50, 60, 70, 80, 90, 100, 150, 200, 300, and 400 μM) in 20 mM TRIS (pH = 8.0) at 37 °C; (b) resolution of fluorescence against the Ni^{2+} concentrations; (c) linear relationship between the fluorescence intensity and Ni^{2+} concentrations (0−50 μM); and (d) selectivity of Ni^{2+} (300 μM) and coexisting metal ions (500 μM). Error bars displayed the standard deviation for three individual tests.

time, and the pH condition, as revealed in Figure 9. Before testing the sensor, the stability of the Y-shaped DNAzyme was determined with the help of the emission spectra consisting of the FAM, ROX, and TAMRA fluorophores. Figure 9a indicates that the fluorescence intensity of the three dissimilar fluorophores was nearly stable at a 1:1:1 ratio for 2 h, implying the enhanced stability of the Y-shaped DNA structure. When the ratio of the DNAzymes was 1:1:1, the structure influenced the stability of the Y-shaped DNAzyme. Subsequently, the amount of DNAzyme became a sensitive measurement for this biosensor. Next, we optimized the stability of the Y-shaped DNAzyme by monitoring the fluorescence intensity changes of the three fluorophores. Figure 9b shows that the fluorescence intensities of the three fluorophores were relatively stable for 2 h, which indicated the stability of the formed Y-shaped DNAzyme structure. The influence of the concentration of the DNAzymes on the fluorescence intensity with and without the target metal ions (Hg^{2+}, Ni^{2+}, and Ag^{+}) was studied, as revealed in Figure 9c. In this optimization study, we used the Hg^{2+}-dependent DNAzyme as an example. In the absence of the Hg^{2+} ion, the fluorescence intensity of FAM increased with increasing DNAzyme concentration owing to the increased amount of the FAM fluorophore. However, in the presence of a Hg^{2+} ion, the fluorescence intensity of FAM significantly decreased as a result of the adsorption of cleaved FAM-labeled SA on the surface of the MOF-MoS_2NBs. Accordingly, the concentration of the three DNAzymes was optimized within 5−200 nM. The experimental results demonstrated that the fluorescence emissions attained maximum levels when the concentration of the DNAzyme was at 150 nM. However, the concentration of DNAzymes greater than 150 nM did not influence the sensing ability. Moreover, we also optimized another two DNAzymes using the above-mentioned procedure. The influences of the pH and the incubation time are also optimized in Figure 9d,e. The sensing mechanism demonstrated that the fluorescence quenching steps include two stages: the cleavage reaction of the DNAzyme and the adsorption of the fluorophore-labeled SA portion on the MOF-MoS_2NB surface. In addition, pH is a crucial parameter for the DNAzyme cleavage reaction. Also, the DNAzyme activity cleavage was greatly affected by the pH of the solution. Therefore, the influence of pH (Tris−HCl) on the three kinds of DNAzyme is optimized in Figure 9d. As a result, the activity of the DNAzyme was higher at pH 8. When the pH was increased above 8, the activity of the DNAzyme did not change. This signified that the activity of the DNAzyme was highly pH-dependent. Thus, a pH value of 8.0 was suitable for the sensing system. As shown in Figure 9e, the Hg^{2+}, Ni^{2+}, and Ag^{+} ions steadily decreased the fluorescence intensity during the reaction time and then existed as a plateau for 25 min. According to the evidence,[48] the DNAzyme cleavage process typically ended in 5 min due to the high reaction efficacy. Consequently, the adsorption stage functioned as a rate-limiting process for the overall reaction, which culminated in a longer response time. The reliability of the incubation time with these metal ions indicated that simultaneous detection was achievable.

3.6. Analytical Performance. *3.6.1. Sensitivity and Specificity.* The sensitivity response of the fluorescence

https://doi.org/10.1021/acsami.1c07086
ACS Appl. Mater. Interfaces 2021, 13, 31710−31724

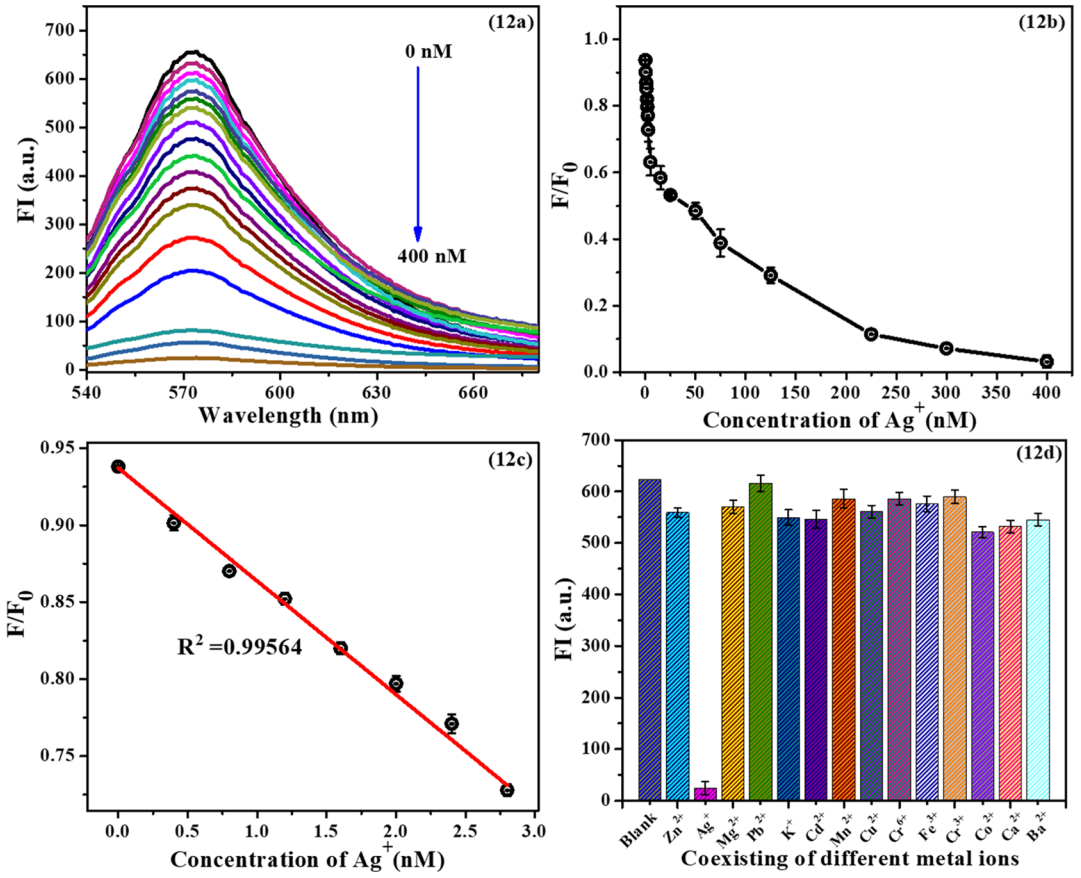

Figure 12. (a) Fluorescence spectra for Ag^+ MOF-MoS_2NBs (25 $\mu g \cdot mL^{-1}$) and Y-shaped DNAzyme (20 μM) at various concentrations (0, 0.4, 0.8, 1.2, 1.6, 2, 2.4, 2.8, 5, 15, 25, 50, 75, 125, 225, 300, and 400 nM) in 20 mM TRIS (pH = 8.0) at 37 °C; (b) resolution of fluorescence against the Ag^+ concentrations; (c) linear relationship between the fluorescence intensity and Ag^+ concentrations (0−3.0 nM); and (d) selectivity of Ag^+ (300 nM) and coexisting metal ions (1000 nM). Error bars displayed the standard deviation for three individual tests.

Table 1. Comparison of Various Biosensing Probes Used to Determine Hg^{2+}, Ni^{2+}, and Ag^+ Ions[a]

biosensing probe	method	LOD	targets	refs
MOF/DNA	FT	3.0 nM	Hg^{2+}	49
DNA@MOF	FT	3.2 nM	Hg^{2+}	50
DNA/MOF	FT	7.5 and 2.6 nM	Ag^+ and Hg^{2+}	51
DNAzyme	FT	12.9 μM	Ni^{2+}	52
3D MOF/DNAzyme	FT	4.2 nM	Ag^+	53
WS_2 Nanosheets	FT	3.3 nM and 1.2 nM	Hg^{2+} and Ag^+	54
Y-shaped DNAzyme and MOF-MoS2NBs	FT	0.11 nM, 7.8 μM; and 0.25 nM	Hg^{2+}, Ni^{2+}; and Ag^+	this work

[a]FT-Fluorescence Technique.

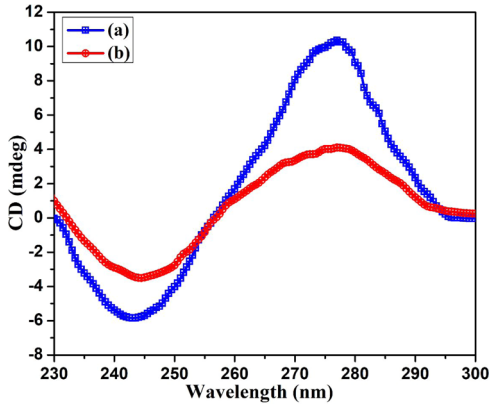

Figure 13. (a) CD spectra for Y-shaped DNAzyme (2 μM) and (b) Y-shaped DNAzyme/MOF-MoS_2NBs (2 μM) with Hg^{2+}, Ni^{2+}, and Ag^+ ions (2 μM).

biosensor was analyzed for the multiple detections of Hg^{2+}, Ni^{2+}, and Ag^+ ions with different concentrations. The effective fluorescence quenching for the cleaved fluorophore-labeled SAs on the MOF-MoS_2NB response to various concentrations of the Hg^{2+}, Ni^{2+}, and Ag^+ metal ions is shown in Figures 10a, 11a, and 12a. We found that the fluorescence intensity of the cleaved fluorophore-labeled SAs was significantly quenched by the MOF-MoS_2NBs. Following this, the fluorescence intensity decreased gradually with increasing concentrations of metal ions, which were recorded under the optimized conditions. In addition, these kinds of metal ions were specifically cleaved to target the DNAzymes. Particularly the thymine-rich (T-rich) and cytosine-rich (C-rich) DNA sequences in the Hg^{2+}zyme and Ag^+zyme and the nitrogen-rich ligand moiety (glycyl−histidine-functionalized tertiary amine) were inserted at the RNA site of the Ni^{2+}zyme. This utilized the T-Hg^{2+}-T, C−Ag^+-C, and the *N*−Ni^{2+}-N coordination chemistry and induced three different types of DNAzymes, which were cleaved (activated) specifically. The cleaved fluorophore-labeled SAs were quenched on the versatile MOF-MoS_2NB surface. The intensity of the fluorescence decreased significantly as the concentration of the Hg^{2+}, Ni^{2+}, and the Ag^+ ions increased

https://doi.org/10.1021/acsami.1c07086
ACS Appl. Mater. Interfaces 2021, 13, 31710−31724

Table 2. Determination of Existence for the Hg^{2+} Ion in RWS Using the Proposed Technique

sample	spiked (nM)	detected ±SD Hg^{2+}	recovery (%) Hg^{2+}
tap water	0.3	$0.311^x \pm 0.47^y$	103.6
	0.6	$0.623^x \pm 0.24^y$	103.8
	0.9	$0.947^x \pm 0.21^y$	100.5
lake water	0.3	$0.308^x \pm 0.38^y$	102.6
	0.6	$0.592^x \pm 0.42^y$	98.6
	0.9	$0.893^x \pm 0.32^y$	99.2

Table 3. Determination of Existence for the Ni^{2+} Ion in RWS Using the Proposed Technique

sample	spiked (μM)	detected ±SD Ni^{2+}	recovery (%) Ni^{+}
tap water	10	$10.231^x \pm 0.35^y$	102.3
	15	$15.533^x \pm 0.53^y$	103.5
	20	$20.337^x \pm 0.21^y$	101.6
lake water	10	$10.427^x \pm 0.33^y$	104.2
	15	$14.982^x \pm 0.42^y$	99.8
	20	$19.883^x \pm 0.32^y$	99.4

Table 4. Determination of Existence for the Ag^{+} Ion in RWS Using the Proposed Technique[a]

sample	spiked (nM)	detected ±SD Ag^{+}	recovery (%) Ag^{+}
tap water	0.4	$0.421^x \pm 0.45^y$	105.2
	0.8	$0.813^x \pm 0.33^y$	101.6
	1.2	$1.207^x \pm 1.21^y$	100.5
Lake water	0.4	$0.408^x \pm 0.38^y$	102.1
	0.8	$0.792^x \pm 0.42^y$	99.1
	1.2	$1.193^x \pm 1.32^y$	99.4

[a] x-mean values of three determinations, y-standard deviation.

from 0 to 300 nM, 0 to 400 μM, and 0 to 400 nM, respectively, as shown in Figures 10b, 11b, and 12b. As a result, the virtuous linearity was achieved between the concentration of the metal ions and the fluorescence intensity from 0 to 1.6 nM (R^2 = 0.99808) for Hg^{2+} (Figure 10c), 0 to 50 μM (R^2 = 0.98748) for Ni^{2+} (Figure 11c), and 0 to 3 nM (R^2 = 0.99564) for Ag^{+} (Figure 12c). The limits of detection were found to be 0.11 nM for Hg^{2+}, 7.8 μM for Ni^{2+}, and 0.25 nM for Ag^{+}, which were obtained as 3 times the standard deviation of the blank, respectively. These results indicate that this MOF-MoS_2NB nanomaterial possessed remarkable quenching efficiency, high sensitivity, and selectivity for the detection of Hg^{2+}, Ni^{2+}, and Ag^{+} ions when compared to the previous reports generated using the single DNAzyme-based sensors. The advantages of the present sensing protocol were compared with the previously reviewed biosensors, as revealed in Table 1.

3.6.2. Selectivity. The exploration of the selectivity of the proposed sensor was done with other environmentally significant metal ions, including K, Co, Zn, Mn, Ca, Pb, Cd, Fe, Cr, Fe, Cd, Cu, Mg, and Ba. In a typical experiment, one of these metal ions was added to the Y-shaped DNAzyme/MOF-MoS_2NB complex at a final concentration of 20 min. As shown in Figures 10d, 11d, and 12d, the fluorescence emmision was significantly decreased by Hg^{2+}, Ni^{2+}, and Ag^{+} ions when compared to the other interfering metal ions. Hence, these target metal ions selectively responded to high catalytic activity, and no obvious response was observed during the addition of the co-interfering metal ions. These results indicated that the proposed strategy had a reasonable selectivity, which could be used successfully in the detection of the Hg^{2+}, Ni^{2+}, and Ag^{+} ions.

3.7. Scrutiny of CDS. Here, the performance of the Y-shaped DNAzyme was collectively analyzed using the three types of DNAzymes, which were Hg^{2+}zyme, Ni^{2+}zyme, and Ag^{+}zyme. They possessed different DNA sequences which were easy to detect and rapid. The Hg^{2+}, Ni^{2+}, and Ag^{+} ion detection sensors used CDS. The detection of Hg^{2+}, Ni^{2+}, and Ag^{+} ions was performed based on the degree of absorption induced by the right- and left-handed circularly polarized light (ΔA) for the Hg^{2+}, Ni^{2+}, and Ag^{+} ions during the cleavage of the Y-shaped DNAzyme. The specific wavelength of the absorption peak was determined according to the structure of the Y-shaped DNAzyme, which was simultaneously cleaved by the Hg^{2+}, Ni^{2+}, and Ag^{+} ions. The application of multiple metal ions as sensors using CDS was never reported in previous works of literature.

The sensing mechanism was scrutinized for affirmation using the CDS. The DNA structural conformation changes observed in the Y-shaped DNAzyme were triggered by the Hg^{2+}, Ni^{2+}, and Ag^{+} ions. Figure 13a reveals an obvious cotton effect, which indicated the peak of the Y-shaped DNAzyme with a concentration of 2 μM. A high positive CDS peak at 276 nm and a broad negative peak at 243 nm were observed, which attributed to the characteristic peaks of the Y-shaped DNAzyme. When the targets (Hg^{2+}, Ni^{2+}, and Ag^{+} ions) were added to the sensing complex(Y-shaped DNAzyme/MOF-MoS_2NBs), the positive and negative peaks underwent an unanticipated decrease because these targets could be cleaved onto the three kinds of RNA sites of the Y-shaped DNAzyme which liberated the SA fragments with fluorophores (ssDNA), as shown in Figure 13b.

3.8. Application in Real Water Samples. The designed Y-shaped DNAzyme/MOF-MoS_2NB sensing probes established the practical applicability by determining the Hg^{2+}, Ni^{2+}, and Ag^{+} ions in real water samples using the standard addition method. The real samples were adjusted with 10 mM Tris−HCl (pH 8.0) before the analysis. Briefly, the real water samples were diluted three times using 10 mM Tris−HCl and spiked with 0.1 M metal ions (Hg^{2+}, Ni^{2+}, and Ag^{+} ions) separately. Furthermore, these samples were used for the analysis of the fluorescence measurement and also for the detection of the Hg^{2+}, Ni^{2+}, and Ag^{+} ions for establishing the accuracy of the proposed method. The recovery values of the water samples are summarized in Tables 2−4. It can be observed that the proposed sensor retained the recovery range from 98.6 to 104.0% (Hg^{2+}), 99.0 to 103.5% (Ni^{2+}), and 99.1 to 105.2% (Ag^{+}), respectively. This outcome reveals that the Y-shaped DNAzyme/MOF-MoS_2NB sensor was found to be suitable for the determination of Hg^{2+}, Ni^{2+}, and Ag^{+} ions in a real water sample with appropriate recoveries for practical application. Furthermore, the reproducibility was investigated by measuring the target metal ions for repetitive samples. The RSDs (tap and lake water) were 0.9 and 2.4% for Hg^{2+}, 0.1 and 3.4% for Ni^{2+}, and 2.7 and 1.9% for Ag^{+}, respectively. These results revealed that the proposed strategy possessed good selectivity and reproducibility and hence can be successfully used in the simultaneous detection of the Hg^{2+}, Ni^{2+}, and Ag^{+} ions.

https://doi.org/10.1021/acsami.1c07086
ACS Appl. Mater. Interfaces 2021, 13, 31710−31724

4. CONCLUSIONS

As a summation, this investigation reveals the enhanced catalytic activity of the Y-shaped DNAzyme and the 3D MOF-MoS_2NBs used in the development of fluorescent biosensors and their application in the simultaneous detection of Hg^{2+}, Ni^{2+}, and Ag^{+} ions in the aqueous media. Interestingly, the circular cleavages of the three distinct fluorophore (FAM, ROX, and TAMRA)-labeled Y-shaped DNAzymes were found to possess an enhanced sensitivity and enabled the simultaneous detection of the Hg^{2+}, Ni^{2+}, and Ag^{+} ions, which was definitely superior to the previously reported sensing systems. Under the optimized conditions, the analytical performance of the developed biosensor exhibited an excellent selectivity toward Hg^{2+}, Ni^{2+}, and Ag^{+} even in the presence of other coexisting metal ions whose detection limits were found to be 0.11 nM, 7.8 μM, and 0.25 nM, respectively. The excellent performance of the present technique used in the detection of the Hg^{2+}, Ni^{2+}, and Ag^{+} ions in real water samples was completely justified with satisfactory results. Moreover, the multiple detection capabilities will significantly minimize the time and sensor costs which are pretty remarkable. The investigation paves the way for excellent prospects in practical applications in the detection and imaging of multiple metal ions in environmental and clinical samples under the complete utilization of the proposed sensor.

AUTHOR INFORMATION

Corresponding Author

Panneerselvam Perumal − *Department of Chemistry, SRM Institute of Science and Technology, Kattankulathur 603 203 Tamil Nadu, India;* orcid.org/0000-0003-2647-6835; Phone: +91 9688538842; Email: panneerp1@srmist.edu.in, panneerchem82@gmail.com

Authors

Rajaji Pavadai − *Department of Chemistry, SRM Institute of Science and Technology, Kattankulathur 603 203 Tamil Nadu, India*

Arunjegan Amalraj − *Department of Chemistry, SRM Institute of Science and Technology, Kattankulathur 603 203 Tamil Nadu, India*

Sivanesan Subramanian − *Department of Applied Science and Technology, A.C Technology, Anna University, Chennai 600 025, India;* orcid.org/0000-0002-2103-4862

Complete contact information is available at: https://pubs.acs.org/10.1021/acsami.1c07086

Notes

The authors declare no competing financial interest.

ACKNOWLEDGMENTS

The authors acknowledge the financial support from the Department of Chemistry, SRM Institute of Science and Technology, Tamil Nadu-603 203, India.

REFERENCES

(1) Choudhury, N.; Ruidas, B.; Mukhopadhyay, C. D.; De, P. Rhodamine-Appended Polymeric Probe: An Efficient Colorimetric and Fluorometric Sensing Platform for Hg^{2+} in Aqueous Medium and Living Cells. *ACS Appl. Polym. Mater.* **2020**, *2*, 5077−5085.

(2) Treto-Suárez, MA.; Tapia, J.; Hidalgo-Rosa, Y.; Páez-Hernández, D.; Molins, E.; Zarate, X.; Schott, E. New Sensitive and Selective Chemical Sensors for Ni^{2+} and Cu^{2+} Ions: Insights into the Sensing Mechanism through DFT Methods. *J. Phys. Chem. A* **2020**, *124*, 6493−6503.

(3) Shen, F.; Mao, S.; Mathivanan, J.; Wu, Y.; Chandrasekaran, A. R.; Liu, H.; Gan, J.; Sheng, J. Short DNA Oligonucleotide as a Ag^{+} Binding Detector. *ACS Omega* **2020**, *5*, 28565−28570.

(4) Tutschku, S.; Schantz, M. M.; Wise, S. A. Determination of methylmercury and butyltin compounds in marine biota and sediments using microwave-assisted acid extraction, solid-phase microextraction, and gas chromatography with microwave-induced plasma atomic emission spectrometric detection. *Anal. Chem.* **2002**, *74*, 4694−4701.

(5) Da Silva, M. J.; Paim, A. P.; Pimentel, M. F.; Cervera, M. L.; De la Guardia, M. Determination of mercury in rice by cold vapor atomic fluorescence spectrometry after microwave-assisted digestion. *Anal. Chim. Acta* **2010**, *667*, 43−48.

(6) Date, Y.; Aota, A.; Terakado, S.; Sasaki, K.; Matsumoto, N.; Watanabe, Y.; Matsue, T.; Ohmura, N. Trace-level mercury ion (Hg^{2+}) analysis in aqueous sample based on solid-phase extraction followed by microfluidic immunoassay. *Anal. Chem.* **2013**, *85*, 434−440.

(7) Asfaram, A.; Ghaedi, M.; Ghezelbash, G. R. Biosorption of Zn^{2+}, Ni^{2+} and Co^{2+} from water samples onto Yarrowia lipolytica ISF7 using a response surface methodology, and analyzed by inductively coupled plasma optical emission spectrometry (ICP-OES). *RSC Adv.* **2016**, *6*, 23599−23610.

(8) Soylak, M.; Kars, A.; Narin, I. Coprecipitation of Ni^{2+}, Cd^{2+} and Pb^{2+} for preconcentration in environmental samples prior to flame atomic absorption spectrometric determinations. *J. Hazard. Mater.* **2008**, *159*, 435−439.

(9) Thulasidas, S. K.; Kulkarni, M. J.; Porwal, N. K.; Page, A. G.; Sastry, M. D. Direct determination of beryllium, cadmium, lithium, lead and silver in thorium nitrate solution by electrothermal atomization atomic absorption spectrometry. *Anal. Lett.* **1988**, *21*, 265−278.

(10) Ganjali, M. R.; Daftari, A.; Hajiagha-Babaei, L.; Badiei, A.; Saberyan, K.; Ziarani, G. M.; Moghimi, A. Pico level monitoring of silver with modified hexagonal mesoporous compound (MCM-41) and inductively coupled plasma atomic emission spectrometry. *Water, Air, Soil Pollut.* **2006**, *173*, 71−80.

(11) Vacchina, V.; Mari, S.; Czernic, P.; Marquès, L.; Pianelli, K.; Schaumlöffel, D.; Lebrun, M.; Łobiński, R. Speciation of nickel in a hyperaccumulating plant by high-performance liquid chromatography− inductively coupled plasma mass spectrometry and electrospray MS/MS assisted by cloning using yeast complementation. *Anal. Chem.* **2003**, *75*, 2740−2745.

(12) Yao, J.; He, Y.; Li, L.; LiYang, P. M. Magnified Fluorescent Aptasensors Based on a Gold Nanoparticle− DNA Hybrid and DNase I for the Cycling Detection of Mercury (II) Ions in Aqueous Solution. *Ind. Eng. Chem. Res.* **2019**, *58*, 21201−21207.

(13) Saha, U.; Chatterjee, S.; Dolai, M.; Suresh Kumar, G. Biophysical and Thermodynamic Investigations on the Differentiation of Fluorescence Response towards Interaction of DNA: A Pyrene-Based Receptor versus Its Fe (III) Complex. *ACS Appl. Bio Mater.* **2020**, *3*, 7810−7820.

(14) Wu, Y.; Yue, Y.; Deng, S.; He, G.; Gao, H.; Zhou, M.; Zhong, K.; Deng, R. Ratiometric-enhanced G-Quadruplex Probes for Amplified and Mix-to-Read Detection of Mercury Pollution in Aquatic Products. *J. Agric. Food Chem.* **2020**, *68*, 12124−12131.

(15) Arunjegan, A.; Rajaji, P.; Sivanesan, S.; Panneerselvam, P. A Turn-ON fluorometric biosensor based on ssDNA immobilized with a metal phenolic nanomaterial for the sequential detection of Pb (ii) and epirubicin cancer drug. *RSC Adv.* **2021**, *11*, 12361−12373.

(16) Moon, W. J.; Liu, J. Interfacing Catalytic DNA with Nanomaterials. *Adv. Mater. Interfaces* **2020**, *7*, 2001017.

(17) Feng, M.; Gu, C.; Sun, Y.; Zhang, S.; Tong, A.; Xiang, Y. Enhancing catalytic activity of uranyl-dependent DNAzyme by flexible linker insertion for more sensitive detection of uranyl ion. *Anal. Chem.* **2019**, *91*, 6608−6615.

(18) Shi, X.; Meng, H. M.; Geng, X.; Qu, L.; Li, Z. DNAzyme−Metal−Organic Framework Two-Photon Nanoprobe for In situ Monitoring of Apoptosis-Associated Zn^{2+} in Living Cells and Tissues. *ACS Sens.* **2020**, *5*, 3150−3157.
(19) Yin, Y.; Chen, G.; Gong, L.; Ge, K.; Pan, W.; Li, N.; Machuki, J. O.; Yu, Y.; Geng, D.; Dong, H.; Gao, F. DNAzyme-powered three-dimensional DNA walker nanoprobe for detection amyloid β-peptide oligomer in living cells and in vivo. *Anal. Chem.* **2020**, *92*, 9247−9256.
(20) Hwang, K.; Mou, Q.; Lake, R. J.; Xiong, M.; Holland, B.; Lu, Y. Metal-dependent DNAzymes for the quantitative detection of metal ions in living cells: recent progress, current challenges, and latest results on FRET ratiometric sensors. *Inorg. Chem.* **2019**, *58*, 13696−13708.
(21) Yang, Z.; Loh, K. Y.; Chu, Y. T.; Feng, R.; Satyavolu, N. S.; Xiong, M.; Nakamata Huynh, S. M.; Hwang, K.; Li, L.; Xing, H.; Zhang, X. Optical control of metal ion probes in cells and zebrafish using highly selective DNAzymes conjugated to upconversion nanoparticles. *J. Am. Chem. Soc.* **2018**, *140*, 17656−17665.
(22) Peng, D.; Li, Y.; Huang, Z.; Liang, R. P.; Qiu, J. D.; Liu, J. Efficient DNA-catalyzed porphyrin metalation for fluorescent ratiometric Pb^{2+} detection. *Anal. Chem.* **2019**, *91*, 11403−11408.
(23) Xiao, M.; Lai, W.; Man, T.; Chang, B.; Li, L.; Chandrasekaran, A. R.; Pei, H. Rationally engineered nucleic acid architectures for biosensing applications. *Chem. Rev.* **2019**, *119*, 11631−11717.
(24) Hu, Y.; Huang, Z.; Liu, B.; Liu, J. Hg (II) Adsorption on Gold Nanoparticles Dominates DNA-Based Label-Free Colorimetric Sensing. *ACS Appl. Nano Mater.* **2021**, *4*, 1377−1384.
(25) Yi, H.; Qin, R.; Ding, S.; Wang, Y.; Li, S.; Zhao, Q.; Pan, F. Structure and Properties of Prussian Blue Analogues in Energy Storage and Conversion Applications. *Adv. Funct. Mater.* **2021**, *31*, 2006970.
(26) Ma, X.; Chang, C.; Zhang, Y.; Niu, P.; Liu, X.; Wang, S.; Li, L. Synthesis of Co-based Prussian Blue Analogues/Dual-Doped Hollow Carbon Microsphere Hybrids as High-Performance Bifunctional Electrocatalysts for Oxygen Evolution and Overall Water Splitting. *ACS Sustainable Chem. Eng.* **2020**, *8*, 8318−8326.
(27) Zhang, X.; Chen, A.; Zhong, M.; Zhang, Z.; Zhang, X.; Zhou, Z.; Bu, X. H. Metal−organic frameworks (MOFs) and MOF-derived materials for energy storage and conversion. *Electrochem. Energy Rev.* **2019**, *2*, 29−104.
(28) Weng, H.; Yan, B. A Eu (III) doped metal-organic framework conjugated with fluorescein-labeled single-stranded DNA for detection of Cu (II) and sulfide. *Anal. Chim. Acta* **2017**, *988*, 89−95.
(29) Wang, C.; Tang, G.; Tan, H. Pyrophosphate ion-triggered competitive displacement of ssDNA from a metal−organic framework and its application in fluorescent sensing of alkaline phosphatase. *J. Mater. Chem. B* **2018**, *6*, 7614−7620.
(30) Yang, Z.; Qian, Y.; Yang, F.; Chen, C.; Tang, X.; Jin, J. Investigating adsorption/desorption of DNA on ZIF-8 surface by fluorescently labeled oligonucleotides. *Langmuir* **2019**, *35*, 16290−16296.
(31) LYang, Q.; Hong, J.; Wu, Y. X.; Cao, Y.; Wu, D.; Hu, F.; Gan, N. A multicolor fluorescence nanoprobe platform using two-dimensional metal organic framework nanosheets and double stirring bar assisted target replacement for multiple bioanalytical applications. *ACS Appl. Mater. Interfaces* **2019**, *11*, 41506−41515.
(32) Zhu, C.; Zeng, Z.; Li, H.; Li, F.; Fan, C.; Zhang, H. Single-layer MoS_2-based nanoprobes for homogeneous detection of biomolecules. *J. Am. Chem. Soc.* **2013**, *135*, 5998−6001.
(33) Lan, L.; Chen, D.; Yao, Y.; Peng, X.; Wu, J.; Li, Y.; Ping, J.; Ying, Y. Phase-dependent fluorescence quenching efficiency of MoS_2 nanosheets and their applications in multiplex target biosensing. *ACS Appl. Mater. Interfaces* **2018**, *10*, 42009−42017.
(34) Chen, W.; Gao, G.; Jin, Y.; Deng, C. A facile biosensor for Aβ40O based on fluorescence quenching of prussian blue nanoparticles. *Talanta* **2020**, *216*, 120930.
(35) Mao, K.; Wu, Z.; Chen, Y.; Zhou, X.; Shen, A.; Hu, J. A novel biosensor based on single-layer MoS_2 nanosheets for detection of Ag^+. *Talanta* **2015**, *132*, 658−663.
(36) Zhao, Y.; Zhang, X.; Wang, C.; Zhao, Y.; Zhou, H.; Li, J.; Jin, H. The synthesis of hierarchical nanostructured MoS_2/Graphene composites with enhanced visible-light photo-degradation property. *Appl. Surf. Sci.* **2017**, *412*, 207−213.
(37) Jia, Q.; Li, Z.; Guo, C.; Huang, X.; Kang, M.; Song, Y.; He, L.; Zhou, N.; Wang, M.; Zhang, Z.; Fu, G. PEGMA-modified bimetallic NiCo Prussian blue analogue doped with Tb (III) ions: Efficiently pH-responsive and controlled release system for anticancer drug. *Chem. Eng. J.* **2020**, *389*, 124468.
(38) Yu, X. Y.; Feng, Y.; Jeon, Y.; Guan, B.; Lou, X. W.; Paik, U. Formation of Ni−Co−MoS2 nanoboxes with enhanced electrocatalytic activity for hydrogen evolution. *Adv. Mater.* **2016**, *28*, 9006−9011.
(39) Ahn, W.; Park, M. G.; Lee, D. U.; Seo, M. H.; Jiang, G.; Cano, Z. P.; Hassan, F. M.; Chen, Z. Hollow Multivoid Nanocuboids Derived from Ternary Ni−Co−Fe Prussian Blue Analog for Dual-Electrocatalysis of Oxygen and Hydrogen Evolution Reactions. *Adv. Funct. Mater.* **2018**, *28*, 1802129.
(40) Guo, Y.; Shu, Y.; Li, A.; Li, B.; Pi, J.; Cai, J.; Cai, H. H.; Gao, Q. Efficient electrochemical detection of cancer cells on in situ surface-functionalized MoS_2 nanosheets. *J. Mater. Chem. B* **2017**, *5*, 5532−5538.
(41) Kristl, M.; Dojer, B.; Gyergyek, S.; Kristl, J. Synthesis of nickel and cobalt sulfide nanoparticles using a low cost sonochemical method. *Heliyon* **2017**, *3*, No. e00273.
(42) Sharma, R.; Iqubal, M.; Jheeta, S. Adsorption and oxidation of aromatic amines on metal (II) hexacyanocobaltate (III) complexes: Implication for oligomerization of exotic aromatic compounds. *Inorganics* **2017**, *5*, 18.
(43) Li, P.; Jiao, Y.; Yao, S.; Wang, L.; Chen, G. Dual role of nickel foam in NiCoAl-LDH ensuring high-performance for asymmetric supercapacitors. *New J. Chem.* **2019**, *43*, 3139−3145.
(44) Yin, X.; Sun, G.; Song, A.; Wang, L.; Wang, Y.; Dong, H.; Shao, G. A novel structure of Ni-(MoS_2/GO) composite coatings deposited on Ni foam under supergravity field as efficient hydrogen evolution reaction catalysts in alkaline solution. *Electrochim. Acta* **2017**, *249*, 52−63.
(45) Wang, G.; Zhang, J.; Lin, S.; Xiao, H.; Yang, Q.; Chen, S.; Yan, B.; Gu, Y. Environmentally friendly nanocomposites based on cellulose nanocrystals and polydopamine for rapid removal of organic dyes in aqueous solution. *Cellulose* **2020**, *27*, 2085−2097.
(46) Mao, Y.; Zhou, B.; Peng, S. Magnetite ultrafine particles/porous reduced graphene oxide in situ grown onto Ni foam as a binder-free electrode for supercapacitors. *RSC Adv.* **2020**, *10*, 20753−20764.
(47) Li, Y.; Chang, K.; Sun, Z.; Shangguan, E.; Tang, H.; Li, B.; Sun, J.; Chang, Z. Selective preparation of 1T-and 2H-Phase MoS2 nanosheets with abundant monolayer structure and their applications in energy storage devices. *ACS Appl. Energy Mater.* **2019**, *3*, 998−1009.
(48) Liu, J.; Lu, Y. A DNAzyme catalytic beacon sensor for paramagnetic Cu^{2+} ions in aqueous solution with high sensitivity and selectivity. *J. Am. Chem. Soc.* **2007**, *129*, 9838−9839.
(49) Chen, H. L.; Li, R. T.; Wu, K. Y.; Hu, P. P.; Zhang, Z.; Huang, N. H.; Zhang, W. H.; Chen, J. X. Experimental and theoretical validations of a one-pot sequential sensing of Hg^{2+} and biothiols by a 3D Cu-based zwitterionic metal−organic framework. *Talanta* **2020**, *210*, 120596.
(50) Hu, P. P.; Liu, N.; Wu, K. Y.; Zhai, L. Y.; Xie, B. P.; Sun, B.; Duan, W. J.; Zhang, W. H.; Chen, J. X. Successive and specific detection of Hg^{2+} and I^- by a DNA@ MOF biosensor: experimental and simulation studies. *Inorg. Chem.* **2018**, *57*, 8382−8389.
(51) Huang, N. H.; Liu, Y.; Li, R. T.; Chen, J.; Hu, P. P.; Young, D. J.; Chen, J. X.; Zhang, W. H. Sequential Ag^+/biothiol and synchronous Ag^+/Hg^{2+} biosensing with zwitterionic Cu^{2+}-based metal−organic frameworks. *Analyst* **2020**, *145*, 2779−2788.
(52) Ren, W.; Huang, P. J.; de Rochambeau, D.; Moon, W. J.; Zhang, J.; Lyu, M.; Wang, S.; Sleiman, H.; Liu, J. Selection of a metal

ligand modified DNAzyme for detecting Ni^{2+}. *Biosens. Bioelectron.* **2020**, *165*, 112285.
(53) Rajaji, P.; Panneerselvam, P. A Novel Polydopamine Grafted 3D MOF Nanocubes Mediated GR-5/GC DNAzyme Complex with Enhanced Fluorescence Emission Response toward Spontaneous Detection of Pb (II) and Ag (I) Ions. *ACS Omega* **2020**, *5*, 25188−25198.
(54) Zuo, X.; Zhang, H.; Zhu, Q.; Wang, W.; Feng, J.; Chen, X. A dual-color fluorescent biosensing platform based on WS_2 nanosheet for detection of Hg^{2+} and Ag^{+}. *Biosens. Bioelectron.* **2016**, *85*, 464−470.

https://doi.org/10.1021/acsami.1c07086
ACS Appl. Mater. Interfaces 2021, 13, 31710−31724